J. Appl. Comput. Mech., 7(3) (2021) 1514-1526
DOI: 10.22055/JACM.2020.35227.2603

ISSN: 2383-4536
jacm.scu.ac.ir

Shahid Chamran University of Ahvaz

Journal of Applied and Computational Mechanics

Research Paper

On Stokes' Second Problem for Burgers' Fluid over a Plane Wall

Safia Akram[1], Asia Anjum[2], Masood Khan[3], Anwar Hussain[3]

[1] MCS, National University of Sciences and Technology, Islamabad, Pakistan
[2] Department of Computer Science, National University of Modern Languages, H-9, Islamabad, Pakistan
[3] Department of Mathematics, Quaid-i-Azam University, Islamabad 44000, Pakistan

Received September 29 2020; Revised November 04 2020; Accepted for publication November 10 2020.
Corresponding author: S. Akram (drsafiaakram@mcs.edu.pk; drsafiaakram@gmail.com)

Abstract. The Stokes' second problem for a Burgers' fluid over a plane wall is considered in this paper. The motion of the fluid is induced by the oscillation of the plane wall between two side walls perpendicular to the plane wall. The exact analytical solutions for the velocity field and the adequate shear stress are established in simple forms by means of integral transforms. The solutions that have been obtained, presented as a sum of the steady and the transient solutions, satisfy all imposed initial and boundary conditions. In the absence of the side walls they reduce to the similar solutions over an infinite plate. Finally, the results for the velocity, as well as a comparison between models, are displayed graphically for pertinent parameters to show interesting aspects of the solutions. It is observed that the velocity and the boundary layer thickness were observed to be decreased in the presence of the side walls. Moreover, the Maxwell fluid was observed to be the speediest and the Newtonian was the slowest.

Keywords: Stokes' second problem; Burgers' fluid; Side walls; Exact solution.

1. Introduction

The present trend in the field of non-Newtonian fluid mechanics is because of many important industrial fluids are non-Newtonian in their flow characteristics and are referred to as rheological fluids. There are numerous examples of non-Newtonian fluids in nature, for instance, lubricants, liquid crystals, paints, foams, slurries, blood, biological fluids, polymer solutions and melts and so forth. The rheological behaviors of non-Newtonian fluids include the ability of the fluid to shear thinning/thickening, the ability of the fluid to exhibit relaxation, the ability of the fluid to creep, the ability of the fluid to yield stress, the presence of the fluid to non-zero normal stress differences and many others. Such rheological characteristics of a fluid are important in evaluating the ability of a fluid to perform a specific function. Non-Newtonian fluids are a broad class of fluids in which the relation connecting the shear stress and shear rate is nonlinear. Hence, no single constitutive relation possesses the potential to predict all kinds of rheological characteristics of non-Newtonian fluids. Consequently, several mathematical models have been developed to describe the shear stress/shear rate relationship of non-Newtonian fluids. Hence, due to the practical and fundamental association of non-Newtonian fluids to industrial applications several investigations [1-10] regarding these fluids are made.

Due to the complex and non-linear behaviors of non-Newtonian fluids, many models like the differential, the rate and the integral types are accorded in the literature. Amongst them, the rate type fluids are those which consider the elastic and memory effects. One of the rate type fluid models developed by Burgers' [11] to describe the behavior of fluids is the model of choice to characterize the response of a variety of geological materials. Burgers' model is the preferred model to describe the response of asphalt and asphalt concrete [12]. This model is also used to model other geological structures like Olivine rocks [13] and the propagation of seismic waves in the interior of earth [14]. It is also widely used in calculating the transient creep property of earth mantle and specifically related to the post-glacial uplift. However, the Burgers' model has not received much attention despite its diverse applications and limited studies [15-23] have been reported on the flows of Burgers' fluid.

Owing to the non-linear equation of state for non-Newtonian fluids, the resulting governing equations are much more complicated in the form of their Newtonian counterparts and therefore, numerical solutions have often been sought. However, in contrast to the numerical studies, the progress has been limited until recent times and exact solutions are not available to many problems of practical interest. These exact solutions even become rare if the constitutive equations of non-Newtonian fluids are considered. The exact solutions are essential for a few reasons. These solutions, if available, facilitate the verification of numerical solvers. They also provide accuracy checks for experimental methods. We mention here some recent attempts [24-40] regarding flows of non-Newtonian fluids. However, compared with the Newtonian fluids, the non-Newtonian fluids usually have more complicated constitutive equations, which bring more difficulties in studying Burgers' fluid flows with analytical methods.

The Stokes' second problem for a Burgers fluid over a plane wall is considered in this research article. The motion of the fluid is induced by the oscillation of the plane wall between two side walls perpendicular to the plane wall. The exact analytical solutions

Published online: February 18 2021

for the velocity field and the adequate shear stress are established in simple forms by means of integral transforms. The solutions that have been obtained, presented as a sum of the steady and the transient solutions, satisfy all imposed initial and boundary conditions. It is worth pointing out that, in the absence of the side walls, they can be easily specialized to those corresponding to the motion over an infinite plate. Finally, the results for the velocity as well as a comparison between models, are displayed graphically for pertinent parameters to show interesting aspects of the solutions. It is hoped that the results obtained will not only provide useful information for applications, but also serve as a complement to the previous studies.

2. Materials and methods

In the absence of body forces, the equations governing the flow of an incompressible fluid are

$$\operatorname{div}\mathbf{V} = 0, \tag{1}$$

$$\rho\left(\frac{\partial \mathbf{V}}{\partial t} + (\mathbf{V}.\nabla)\mathbf{V}\right) = -\nabla p + \operatorname{div}\mathbf{S}, \tag{2}$$

where $\mathbf{V}$ is the velocity field, ρ the density, p the pressure and ∇ represents the gradient operator. The extra stress tensor $\mathbf{S}$ for an incompressible Burgers' fluid is of the following [22]

$$\mathbf{S} + \lambda\frac{D\mathbf{S}}{Dt} + \gamma\frac{D^2\mathbf{S}}{Dt^2} = \mu\left(\mathbf{A} + \lambda_r\frac{D\mathbf{A}}{Dt}\right), \tag{3}$$

with

$$\frac{D\mathbf{S}}{Dt} = \frac{d\mathbf{S}}{dt} - \mathbf{LS} - \mathbf{SL}^T, \tag{4}$$

in which μ is the dynamic viscosity, λ the relaxation time, $\lambda_r(<\lambda)$ the retardation time, γ the material constant of Burgers' fluid, $\mathbf{A} = \mathbf{L} + \mathbf{L}^T$ the first Rivlin Ericksen tensor and $\mathbf{L}$ the velocity gradient.
For the problem under consideration, we assume a velocity field $\mathbf{V}$ and an extra stress tensor $\mathbf{S}$ of the form

$$\mathbf{V} = (u(y,z,t),0,0), \quad \mathbf{S} = \mathbf{S}(y,z,t), \tag{5}$$

where $u(y,z,t)$ is the velocity component in x -direction. For such flow, the constraint of incompressibility is automatically satisfied. If the fluid is at rest up to the moment $t=0$, then

$$\mathbf{S}(y,z,0) = \frac{\partial \mathbf{S}(y,z,0)}{\partial t} = \mathbf{0}. \tag{6}$$

Using Eqs. (5) into Eqs. (2) and (3), a straightforward calculation yields the relevant equations as follows

$$\left(1 + \lambda\frac{\partial}{\partial t} + \gamma\frac{\partial^2}{\partial t^2}\right)S_{xy} = \mu\left(1 + \lambda_r\frac{\partial}{\partial t}\right)\frac{\partial u}{\partial y}, \tag{7}$$

$$\left(1 + \lambda\frac{\partial}{\partial t} + \gamma\frac{\partial^2}{\partial t^2}\right)S_{xz} = \mu\left(1 + \lambda_r\frac{\partial}{\partial t}\right)\frac{\partial u}{\partial z}, \tag{8}$$

$$\rho\frac{\partial u(y,z,t)}{\partial t} = -\frac{\partial p}{\partial x} + \frac{\partial S_{xy}}{\partial y} + \frac{\partial S_{xz}}{\partial z}, \tag{9}$$

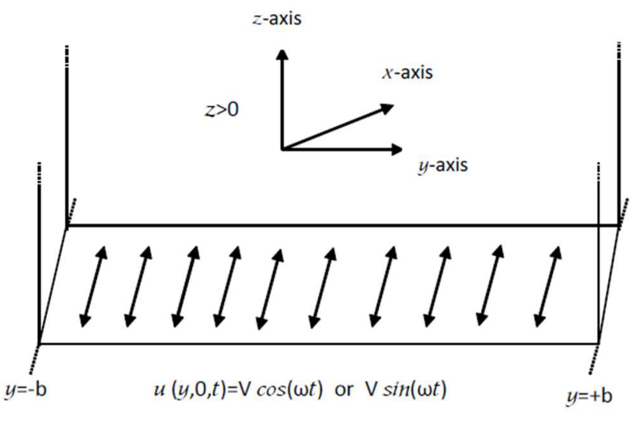

Fig. 1. Incompressible Burgers' fluid over an infinite plate and between two side walls

and $S_{xx}=S_{yz}=S_{yy}=S_{zz}=0$ with S_{xy} and S_{xz} as the non-trivial shear stresses. The elimination of S_{xy} and S_{xz} in Eqs. (7) to (9) results in the governing equation under the form

$$\left(1+\lambda\frac{\partial}{\partial t}+\gamma\frac{\partial^2}{\partial t^2}\right)\frac{\partial u}{\partial t}=-\frac{1}{\rho}\left(1+\lambda\frac{\partial}{\partial t}+\gamma\frac{\partial^2}{\partial t^2}\right)\frac{\partial p}{\partial x}+\nu\left(1+\lambda_r\frac{\partial}{\partial t}\right)\left[\frac{\partial^2 u}{\partial y^2}+\frac{\partial^2 u}{\partial z^2}\right], \tag{10}$$

where $\nu=\mu/\rho$ is the kinematic viscosity of fluid.

3. Description and solution of the problem

Let us consider an incompressible Burgers' fluid at rest over an infinite plate in the $(x,y)-$ plane and between two side walls situated in the planes $y=\pm b$. The side walls are extended to infinity in $x-$ and $z-$ directions. At time $t=0^+$ the plate at $z=0$ starts oscillating in its own plane with the velocity $UH(t)\cos(\omega t)$ or $UH(t)\sin(\omega t)$, where U is the amplitude, ω the angular frequency of the velocity of plate and $H(\cdot)$ denotes the Heaviside unit step function. Owing the shear, the fluid in the channel is gradually moved. Its velocity is of the form (5) and the governing equation are (7), (8) and (10). Assuming that there is no pressure gradient in the flow direction, the relevant problem under initial and boundary conditions is

$$\left(1+\lambda\frac{\partial}{\partial t}+\gamma\frac{\partial^2}{\partial t^2}\right)\frac{\partial u}{\partial t}=\nu\left(1+\lambda_r\frac{\partial}{\partial t}\right)\left[\frac{\partial^2 u}{\partial y^2}+\frac{\partial^2 u}{\partial z^2}\right], \tag{11}$$

$$u(y,z,0)=\frac{\partial u(y,z,0)}{\partial t}=\frac{\partial^2 u(y,z,0)}{\partial t^2}=0, \tag{12}$$

$$u(\pm b,z,t)=0;\quad 0<z<\infty, \tag{13}$$

$$u(y,0,t)=UH(t)\cos(\omega t)\text{ or }UH(t)\sin(\omega t)\quad\text{for all } t, \tag{14}$$

$$u(y,z,t),\quad \frac{\partial u(y,z,t)}{\partial z}\to 0\text{ as } z\to\infty;\quad -b<y<b. \tag{15}$$

The boundary condition (13) suggests that $u(y,z,t)$ can be expressed in the form

$$\frac{u(y,z,t)}{U}=\sum_{n=0}^{\infty}u_n(z,t)\cos(k_n y), \tag{16}$$

where $k_n=(2n+1)\pi/2b$. In order to determine the exact solutions of the above problem, we first use the Fourier sine transform [21]. Substituting the expression (16) in Eq. (11) and employing the Fourier sine transform to the resulting equation together with the accompanying boundary conditions (14) and (15) leads to the equations of the following form

$$\gamma\frac{\partial^3\bar{u}_n(\xi,t)}{\partial t^3}+\lambda\frac{\partial^2\bar{u}_n(\xi,t)}{\partial t^2}+\left[1+\nu\lambda_r\left(\xi^2+k_n^2\right)\right]\frac{\partial\bar{u}_n(\xi,t)}{\partial t}+\nu\left(\xi^2+k_n^2\right)\bar{u}_n(\xi,t)=\frac{4(-1)^n\nu\xi}{(2n+1)\pi}\left[1+\lambda_r\frac{\partial}{\partial t}\right]H(t)\cos(\omega t), \tag{17}$$

respectively,

$$\gamma\frac{\partial^3\bar{u}_n(\xi,t)}{\partial t^3}+\lambda\frac{\partial^2\bar{u}_n(\xi,t)}{\partial t^2}+\left[1+\nu\lambda_r\left(\xi^2+k_n^2\right)\right]\frac{\partial\bar{u}_n(\xi,t)}{\partial t}+\nu\left(\xi^2+k_n^2\right)\bar{u}_n(\xi,t)=\frac{4(-1)^n\nu\xi}{(2n+1)\pi}\left[1+\lambda_r\frac{\partial}{\partial t}\right]H(t)\sin(\omega t), \tag{18}$$

where $\bar{u}_n(\xi,t)$ representing the Fourier sine transform of $u(z,t)$ satisfies the following initial conditions

$$\bar{u}_n(\xi,0)=\frac{\partial\bar{u}_n(\xi,0)}{\partial t}=\frac{\partial^2\bar{u}_n(\xi,0)}{\partial t^2}=0\quad\text{for}\quad\xi>0. \tag{19}$$

Next, we employ the Laplace transform to solve the above problems. Let $\bar{U}_n(\xi,q)=\int_0^\infty\bar{u}_n(\xi,t)e^{-qt}dt$ is the Laplace transform of $\bar{u}_n(\xi,t)$. Consequently, applying the Laplace transform to Eqs. (17) and (18) with the aid of the initial conditions (19) and simplifying, we deduce the following expressions

$$\bar{U}_n(\xi,q)=\frac{4(-1)^n\nu\xi}{(2n+1)\pi}\frac{(1+\lambda_r q)}{\gamma q^3+\lambda q^2+\left[1+\nu\lambda_r\left(\xi^2+k_n^2\right)\right]q+\nu\left(\xi^2+k_n^2\right)}\frac{q}{q^2+\omega^2}, \tag{20}$$

respectively,

$$\bar{U}_n(\xi,q)=\frac{4(-1)^n\nu\xi}{(2n+1)\pi}\frac{(1+\lambda_r q)}{\gamma q^3+\lambda q^2+\left[1+\nu\lambda_r\left(\xi^2+k_n^2\right)\right]q+\nu\left(\xi^2+k_n^2\right)}\frac{\omega}{q^2+\omega^2}. \tag{21}$$

Now, for more suitable presentation of the final results, we rewrite Eqs. (20) and (21) in the equivalent forms

$$\bar{U}_n(\xi,q)=\frac{4(-1)^n\nu\xi}{(2n+1)\pi\gamma}\frac{1}{q}\bar{G}(\xi,q), \tag{22}$$

where

$$\bar{G}(\xi,q)=-\frac{r_{1n}^2\chi_{1n}}{(r_{2n}-r_{1n})(r_{1n}-r_{3n})}\frac{1}{q-r_{1n}}-\frac{r_{2n}^2\chi_{2n}}{(r_{1n}-r_{2n})(r_{2n}-r_{3n})}\frac{1}{q-r_{2n}}-\frac{r_{3n}^2\chi_{3n}}{(r_{3n}-r_{1n})(r_{2n}-r_{3n})}\frac{1}{q-r_{3n}}+\omega^2\psi_{3n}(\xi)\frac{q}{q^2+\omega^2}+\omega\psi_{4n}(\xi)\frac{\omega}{q^2+\omega^2}, \tag{23}$$

respectively,

$$\bar{G}(\xi,q)=-\frac{\omega r_{1n}\chi_{1n}}{(r_{2n}-r_{1n})(r_{1n}-r_{3n})}\frac{1}{q-r_{1n}}-\frac{\omega r_{2n}\chi_{2n}}{(r_{1n}-r_{2n})(r_{2n}-r_{3n})}\frac{1}{q-r_{2n}}-\frac{\omega r_{3n}\chi_{3n}}{(r_{3n}-r_{1n})(r_{2n}-r_{3n})}\frac{1}{q-r_{3n}}-\omega\psi_{4n}(\xi)\frac{q}{q^2+\omega^2}+\omega^2\psi_{3n}(\xi)\frac{\omega}{q^2+\omega^2}, \tag{24}$$

where

$$\chi_{jn}=\frac{(1+\lambda_r r_{jn})}{(r_{jn}^2+\omega^2)},\quad r_{jn}=\zeta_{jn}-\frac{\lambda}{3\gamma},\quad (j=1,2,3)$$

and

$$\zeta_{1n}=\sqrt[3]{-\frac{\psi_{2n}(\xi)}{2}+\sqrt{\frac{\psi_{2n}^2(\xi)}{4}+\frac{\psi_{1n}^3(\xi)}{27}}}+\sqrt[3]{-\frac{\psi_{2n}(\xi)}{2}-\sqrt{\frac{\psi_{2n}^2(\xi)}{4}+\frac{\psi_{1n}^3(\xi)}{27}}},$$

$$\zeta_{2n}=h\sqrt[3]{-\frac{\psi_{2n}(\xi)}{2}+\sqrt{\frac{\psi_{2n}^2(\xi)}{4}+\frac{\psi_{1n}^3(\xi)}{27}}}+h^2\sqrt[3]{-\frac{\psi_{2n}(\xi)}{2}-\sqrt{\frac{\psi_{2n}^2(\xi)}{4}+\frac{\psi_{1n}^3(\xi)}{27}}},$$

$$\zeta_{3n}=h^2\sqrt[3]{-\frac{\psi_{2n}(\xi)}{2}+\sqrt{\frac{\psi_{2n}^2(\xi)}{4}+\frac{\psi_{1n}^3(\xi)}{27}}}+h\sqrt[3]{-\frac{\psi_{2n}(\xi)}{2}-\sqrt{\frac{\psi_{2n}^2(\xi)}{4}+\frac{\psi_{1n}^3(\xi)}{27}}},$$

are the roots of the equation $\zeta^3+\psi_{1n}\zeta+\psi_{2n}=0$ and

$$h=(-1+i\sqrt{3})/2,\quad \psi_{1n}(\xi)=-\frac{\lambda^2}{3\gamma^2}+\frac{1+\nu\lambda_r(\xi^2+k_n^2)}{\gamma},$$

$$\psi_{2n}(\xi)=\frac{2\lambda^3}{27\gamma^3}-\frac{\lambda}{3\gamma}\frac{1+\nu\lambda_r(\xi^2+k_n^2)}{\gamma}+\frac{\nu(\xi^2+k_n^2)}{\gamma},$$

$$\psi_{3n}(\xi)=\left[\lambda_r r_{1n}r_{2n}r_{3n}-\omega^2+r_{1n}(r_{2n}-\lambda_r\omega^2)+r_{2n}(r_{3n}-\lambda_r\omega^2)+r_{3n}(r_{1n}-\lambda_r\omega^2)\right]/(r_{1n}^2+\omega^2)(r_{2n}^2+\omega^2)(r_{3n}^2+\omega^2),$$

$$\psi_{4n}(\xi)=\left[r_{1n}r_{2n}r_{3n}+\lambda_r\omega^4-\omega^2r_{1n}(1+\lambda_r r_{2n})-\omega^2r_{2n}(1+\lambda_r r_{3n})-\omega^2r_{3n}(1+\lambda_r r_{1n})\right]/(r_{1n}^2+\omega^2)(r_{2n}^2+\omega^2)(r_{3n}^2+\omega^2).$$

Inverting Eqs. (23) and (24) by means of the Laplace transform and having in mind the convolution theorem, indeed, determine $\bar{u}_n(\xi,t)$ as

$$\bar{u}_n(\xi,t)=\frac{4(-1)^n\nu\xi}{(2n+1)\pi\gamma}\int_0^t g(\xi,s)ds, \tag{25}$$

where $g(\xi,t)$ is the inverse Laplace transform of $\bar{G}(\xi,q)$ and defined as

$$g(\xi,t)=-\frac{r_{1n}^2\chi_{1n}}{(r_{2n}-r_{1n})(r_{1n}-r_{3n})}e^{r_{1n}t}-\frac{r_{2n}^2\chi_{2n}}{(r_{1n}-r_{2n})(r_{2n}-r_{3n})}e^{r_{2n}t}-\frac{r_{3n}^2\chi_{3n}}{(r_{3n}-r_{1n})(r_{2n}-r_{3n})}e^{r_{3n}t}+\omega^2\psi_{3n}(\xi)\cos(\omega t)+\omega\psi_{4n}(\xi)\sin(\omega t), \tag{26}$$

respectively,

$$g(\xi,t)=-\frac{\omega r_{1n}\chi_{1n}}{(r_{2n}-r_{1n})(r_{1n}-r_{3n})}e^{r_{1n}t}-\frac{\omega r_{2n}\chi_{2n}}{(r_{1n}-r_{2n})(r_{2n}-r_{3n})}e^{r_{2n}t}-\frac{\omega r_{3n}\chi_{3n}}{(r_{3n}-r_{1n})(r_{2n}-r_{3n})}e^{r_{3n}t}-\omega\psi_{4n}(\xi)\cos(\omega t)+\omega^2\psi_{3n}(\xi)\sin(\omega t). \tag{27}$$

Finally, inverting Eq. (25) by means of the Fourier sine transform, we find for $u_n(z,t)$ the following simple expressions

$$u_n(z,t)=\frac{8(-1)^n\nu H(t)}{(2n+1)\pi^2\gamma}\left\{-\int_0^\infty\left[\frac{r_{1n}\chi_{1n}}{(r_{2n}-r_{1n})(r_{1n}-r_{3n})}e^{r_{1n}t}+\frac{r_{2n}\chi_{2n}}{(r_{1n}-r_{2n})(r_{2n}-r_{3n})}e^{r_{2n}t}\right.\right.$$
$$\left.+\frac{r_{3n}\chi_{3n}}{(r_{3n}-r_{1n})(r_{2n}-r_{3n})}e^{r_{3n}t}\right]\xi\sin(\xi z)d\xi+\omega\sin(\omega t)\int_0^\infty\psi_{3n}(\xi)\xi\sin(\xi z)d\xi \tag{28}$$
$$\left.-\cos(\omega t)\int_0^\infty\psi_{4n}(\xi)\xi\sin(\xi z)d\xi\right\},$$

respectively,

$$u_n(z,t)=\frac{8(-1)^n\omega\nu H(t)}{(2n+1)\pi^2\gamma}\left\{-\int_0^\infty\left[\frac{\chi_{1n}}{(r_{2n}-r_{1n})(r_{1n}-r_{3n})}e^{r_{1n}t}+\frac{\chi_{2n}}{(r_{1n}-r_{2n})(r_{2n}-r_{3n})}e^{r_{2n}t}\right.\right.$$
$$\left.+\frac{\chi_{3n}}{(r_{3n}-r_{1n})(r_{2n}-r_{3n})}e^{r_{3n}t}\right]\xi\sin(\xi z)d\xi-\cos(\omega t)\int_0^\infty\psi_{3n}(\xi)\xi\sin(\xi z)d\xi \tag{29}$$
$$\left.-\frac{\sin(\omega t)}{\omega}\int_0^\infty\psi_{4n}(\xi)\xi\sin(\xi z)d\xi\right\}.$$

In view of Eqs. (A4) and (A5) from Appendix, the expressions for the velocity field can be written in the simple forms

$$\frac{u(y,z,t)}{U}=\sum_{n=0}^{\infty}\frac{8(-1)^n\nu H(t)}{(2n+1)\pi^2\gamma}\left\{-\int_0^\infty\left[\frac{r_{1n}\chi_{1n}}{(r_{2n}-r_{1n})(r_{1n}-r_{3n})}e^{r_{1n}t}+\frac{r_{2n}\chi_{2n}}{(r_{1n}-r_{2n})(r_{2n}-r_{3n})}e^{r_{2n}t}\right.\right.$$
$$\left.\left.+\frac{r_{3n}\chi_{3n}}{(r_{3n}-r_{1n})(r_{2n}-r_{3n})}e^{r_{3n}t}\right]\xi\sin(\xi z)d\xi+\frac{\pi}{2}\frac{\gamma}{\nu}e^{-A_nz}\cos(\omega t-B_nz)\right\}\cos(k_ny), \tag{30}$$

respectively,

$$\frac{u(y,z,t)}{U}=\sum_{n=0}^{\infty}\frac{8(-1)^n\omega\nu H(t)}{(2n+1)\pi^2\gamma}\left\{-\int_0^\infty\left[\frac{\chi_{1n}}{(r_{2n}-r_{1n})(r_{1n}-r_{3n})}e^{r_{1n}t}+\frac{\chi_{2n}}{(r_{1n}-r_{2n})(r_{2n}-r_{3n})}e^{r_{2n}t}\right.\right.$$
$$\left.\left.+\frac{\chi_{3n}}{(r_{3n}-r_{1n})(r_{2n}-r_{3n})}e^{r_{3n}t}\right]\xi\sin(\xi z)d\xi+\frac{\pi}{2}\frac{\gamma}{\omega\nu}e^{-A_nz}\sin(\omega t-B_nz)\right\}\cos(k_ny), \tag{31}$$

where A_n and B_n are given through Eqs. (A6) and (A7), respectively. The starting solutions (30) and (31) are written as a sum of the steady-state $u_s(y,z,t)$ and the transient $u_t(y,z,t)$ solutions which describe the motion of the fluid for small and large times. However, for large times, they tend to the steady-state solutions

$$\frac{u_s(y,z,t)}{U}=\sum_{n=0}^{\infty}\frac{4(-1)^n e^{-A_nz}}{(2n+1)\pi}\cos(\omega t-B_nz)\cos(k_ny), \tag{32}$$

respectively,

$$\frac{u_s(y,z,t)}{U}=\sum_{n=0}^{\infty}\frac{4(-1)^n e^{-A_nz}}{(2n+1)\pi}\sin(\omega t-B_nz)\cos(k_ny), \tag{33}$$

which are periodic in time and independent of initial conditions. The non-trivial shear stresses $S_{xy}(y,z,t)$ and $S_{xz}(y,z,t)$ can be immediately determined by introducing Eqs. (30) and (31). In order to obtain the shear stress in the plane parallel to the bottom plate, we need $\tau(y,z,t)=S_{xz}(y,z,t)$. Let $\bar{U}(y,z,q)$ and $\bar{\tau}(y,z,q)$ are the Laplace transforms of $u(y,z,t)$ and $\tau(y,z,t)$, respectively. Hence, the Laplace transform of Eq. (8) with the auxiliary conditions (6) leads to

$$\left.\frac{\bar{\tau}(y,z,q)}{\rho}\right|_{z=0}=\frac{\nu(1+\lambda_r q)}{\gamma q^2+\lambda q+1}\left.\frac{\partial\bar{U}(y,z,q)}{\partial z}\right|_{z=0}, \tag{34}$$

with

$$\frac{\bar{U}(y,z,q)}{U}=\sum_{n=0}^{\infty}\bar{U}_n(z,q)\cos(k_ny), \tag{35}$$

where $\bar{U}_n(z,q)$ is the Laplace transform of $u_n(z,t)$ and can be determined, for instance, by taking the inverse Fourier sine transform of Eq. (20), that is,

$$\bar{U}_n(z,q)=\frac{8(-1)^n}{(2n+1)\pi^2}\int_0^\infty \frac{\nu(1+\lambda_r q)\xi\sin(\xi z)}{\gamma q^3+\lambda q^2+\left[1+\nu\lambda_r\left(\xi^2+k_n^2\right)\right]q+\nu\left(\xi^2+k_n^2\right)}\frac{q}{q^2+\omega^2}d\xi. \tag{36}$$

Introducing Eqs. (35) and (36) in Eq. (34) and applying the inverse Laplace transform, we finally obtain the following expression for the shear stress at the bottom wall

$$\begin{aligned}\frac{\tau(y,z,t)|_{z=0}}{\rho U}=&\sum_{n=0}^{\infty}\frac{8(-1)^n H(t)}{(2n+1)\pi^2\gamma^2}\left\{-\int_0^\infty\left[\frac{r_{1n}\chi_{4n}}{(r_{2n}-r_{1n})(r_{1n}-r_{3n})}e^{r_{1n}t}+\frac{r_{2n}\chi_{5n}}{(r_{1n}-r_{2n})(r_{2n}-r_{3n})}e^{r_{2n}t}+\frac{r_{3n}\chi_{6n}}{(r_{3n}-r_{1n})(r_{2n}-r_{3n})}e^{r_{3n}t}\right]\xi^2 d\xi-\frac{\pi}{2}\frac{\gamma\nu k_n}{r_5-r_4}\left[\frac{r_4(1+\lambda_r r_4)e^{r_4 t}}{(r_4^2+\omega^2)}\right.\right.\\&\left.-\frac{r_5(1+\lambda_r r_5)e^{r_5 t}}{(r_5^2+\omega^2)}\right]-\frac{\pi}{2}\sin(\omega t)\left[A_n+B_n\omega\frac{(\lambda_r-\lambda-\lambda_r\gamma\omega^2)}{1+\omega^2(\lambda_r\lambda-\gamma)}\right]+\frac{\pi}{2}\cos(\omega t)\left[B_n-A_n\omega\frac{(\lambda_r-\lambda-\lambda_r\gamma\omega^2)}{1+\omega^2(\lambda_r\lambda-\gamma)}\right]\Bigg\}\cos(k_n y),\end{aligned} \tag{37}$$

where

$$\chi_{jn}=\frac{\nu^2(1+\lambda_r r_{jn})^2}{(r_{jn}^2+\omega^2)(r_{jn}-r_4)(r_{jn}-r_5)},\quad j=4,5,6\quad\text{and } r_{4,5}=\frac{-\lambda\pm\sqrt{\lambda^2-4\gamma}}{2\gamma}.$$

It is noticed that, similar to the velocity field, the above expression for the shear stress is also written as a sum of the steady-state and transient solutions. Indeed, the associated steady-state shear stress at the bottom wall is

$$\frac{\tau_s(y,z,t)|_{z=0}}{\rho U}=-\sum_{n=0}^{\infty}\frac{4(-1)^n}{(2n+1)\pi\gamma^2}\left\{\sin(\omega t)\left[A_n+B_n\omega\frac{(\lambda_r-\lambda-\lambda_r\gamma\omega^2)}{1+\omega^2(\lambda_r\lambda-\gamma)}\right]-\cos(\omega t)\left[B_n-A_n\omega\frac{(\lambda_r-\lambda-\lambda_r\gamma\omega^2)}{1+\omega^2(\lambda_r\lambda-\gamma)}\right]\right\}\cos(k_n y). \tag{38}$$

3.1 Limiting case $b\to\infty$ (flow over an infinite plate)

It is worthwhile pointing out that in the absence of the side walls, namely when $b\to\infty$, the general solutions obtained above can easily be particularized to give known solutions from the literature or new solutions corresponding to the motion over an infinite plate. Eqs. (30) and (31), for example, take the simplified forms

$$\frac{u(z,t)}{U}=\sum_{n=0}^{\infty}\frac{8(-1)^n\nu H(t)}{(2n+1)\pi^2\gamma}\left\{-\int_0^\infty\left[\frac{r_1\chi_1}{(r_2-r_1)(r_1-r_3)}e^{r_1 t}+\frac{r_2\chi_2}{(r_1-r_2)(r_2-r_3)}e^{r_2 t}+\frac{r_3\chi_3}{(r_3-r_1)(r_2-r_3)}e^{r_3 t}\right]\xi\sin(\xi z)d\xi+\frac{\pi}{2}\frac{\gamma}{\nu}e^{-Az}\cos(\omega t-Bz)\right\}, \tag{39}$$

respectively,

$$\frac{u(z,t)}{U}=\sum_{n=0}^{\infty}\frac{8(-1)^n\omega\nu H(t)}{(2n+1)\pi^2\gamma}\left\{-\int_0^\infty\left[\frac{\chi_1}{(r_2-r_1)(r_1-r_3)}e^{r_1 t}+\frac{\chi_2}{(r_1-r_2)(r_2-r_3)}e^{r_2 t}+\frac{\chi_3}{(r_3-r_1)(r_2-r_3)}e^{r_3 t}\right]\xi\sin(\xi z)d\xi+\frac{\pi}{2}\frac{\gamma}{\omega\nu}e^{-Az}\sin(\omega t-Bz)\right\}, \tag{40}$$

where,

$$\chi_j=\frac{(1+\lambda_r r_j)}{(r_j^2+\omega^2)},\quad r_j=\zeta_j-\frac{\lambda}{3\gamma},\quad (j=1,2,3)$$

and

$$\zeta_1=\sqrt[3]{-\frac{\psi_2(\xi)}{2}+\sqrt{\frac{\psi_2^2(\xi)}{4}+\frac{\psi_1^3(\xi)}{27}}}+\sqrt[3]{-\frac{\psi_2(\xi)}{2}-\sqrt{\frac{\psi_2^2(\xi)}{4}+\frac{\psi_1^3(\xi)}{27}}},$$

$$\zeta_2=h\sqrt[3]{-\frac{\psi_2(\xi)}{2}+\sqrt{\frac{\psi_2^2(\xi)}{4}+\frac{\psi_1^3(\xi)}{27}}}+h^2\sqrt[3]{-\frac{\psi_2(\xi)}{2}-\sqrt{\frac{\psi_2^2(\xi)}{4}+\frac{\psi_1^3(\xi)}{27}}},$$

$$\zeta_3=h^2\sqrt[3]{--\frac{\psi_2(\xi)}{2}+\sqrt{\frac{\psi_2^2(\xi)}{4}+\frac{\psi_1^3(\xi)}{27}}}+h\sqrt[3]{-\frac{\psi_2(\xi)}{2}-\sqrt{\frac{\psi_2^2(\xi)}{4}+\frac{\psi_1^3(\xi)}{27}}},$$

are the roots of the equation $\zeta^3+\psi_1\ \zeta+\psi_2=0$ and

$$\psi_1(\xi)=-\frac{\lambda^2}{3\gamma^2}+\frac{1+\nu\lambda_r\xi^2}{\gamma},\quad \psi_2(\xi)=\frac{2\lambda^3}{27\gamma^3}-\frac{\lambda}{3\gamma}\frac{1+\nu\lambda_r\xi^2}{\gamma}+\frac{\nu\xi^2}{\gamma},$$

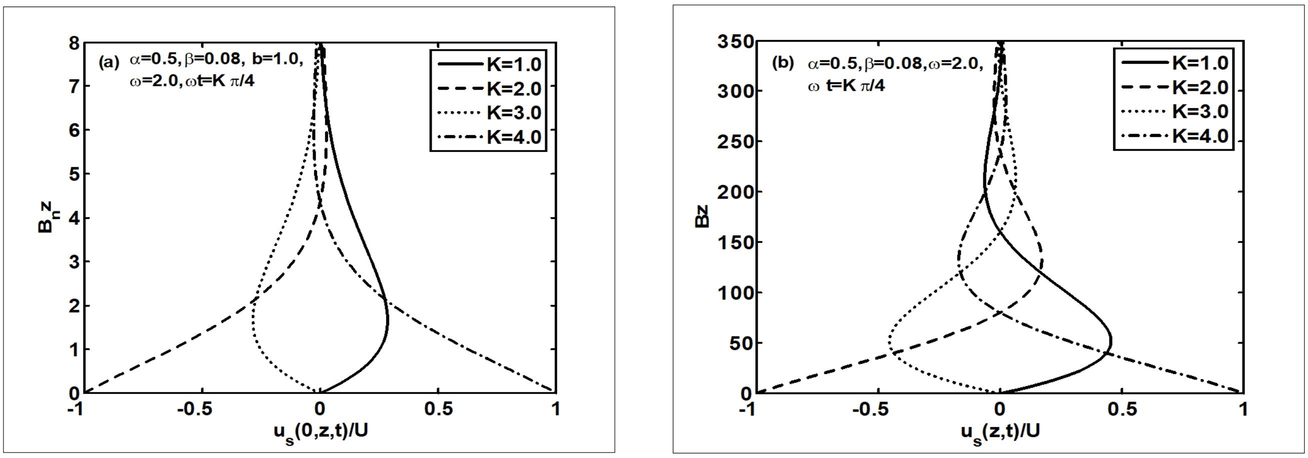

(a) (b)

Fig. 2. Profiles of the velocity u_s/U for different times t for the cosine oscillation: (a) presence of the side walls and (b) absence of the side walls.

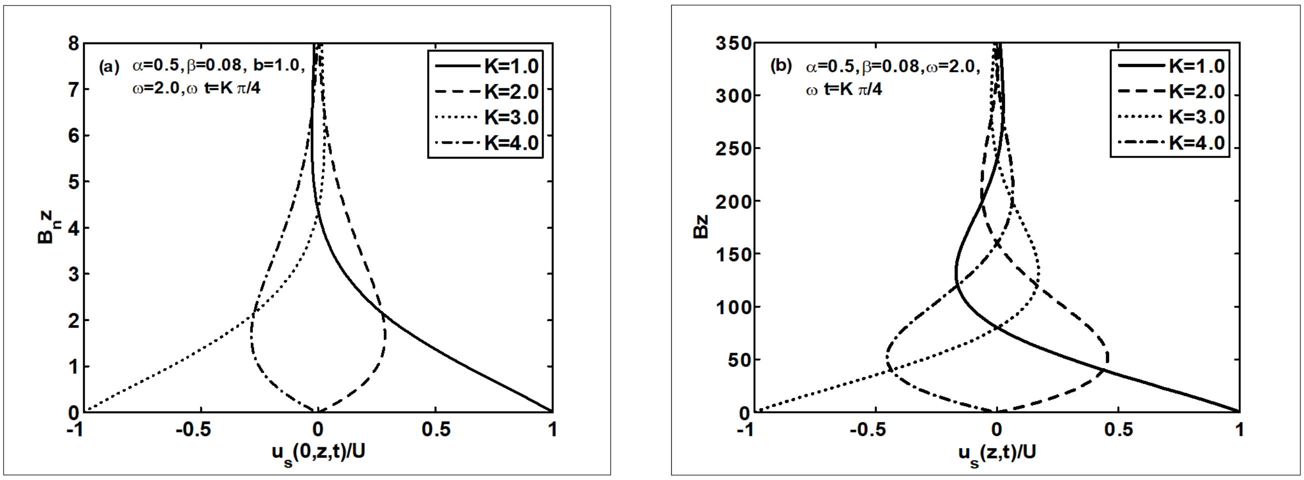

(a) (b)

Fig. 3. Profiles of the velocity u_s/U for different times t for the sine oscillation: (a) presence of the side walls and (b) absence of the side walls.

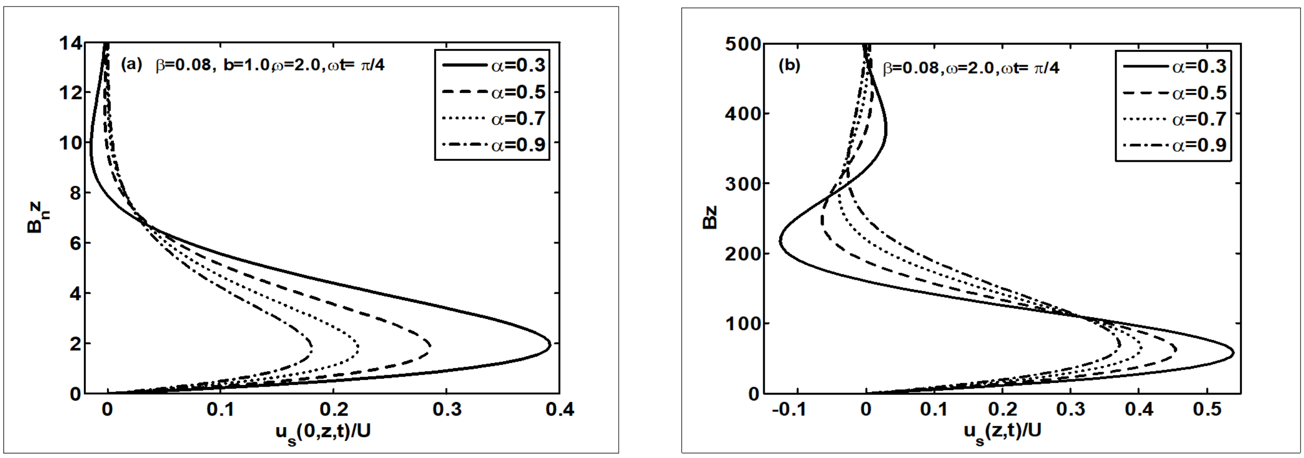

(a) (b)

Fig. 4. Profiles of the velocity u_s/U for different values of the elasticity parameter α for the cosine oscillation: (a) presence of the side walls and (b) absence of the side walls.

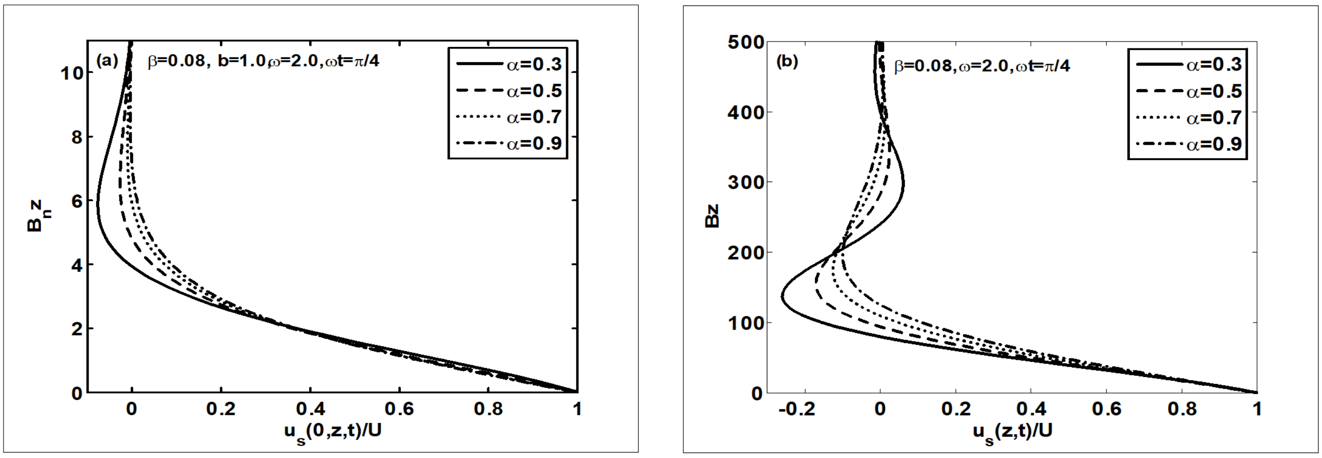

(a) (b)

Fig. 5. Profiles of the velocity u_s / U for different values of the elasticity parameter α for the sine oscillation: (a) presence of the side walls and (b) absence of the side walls.

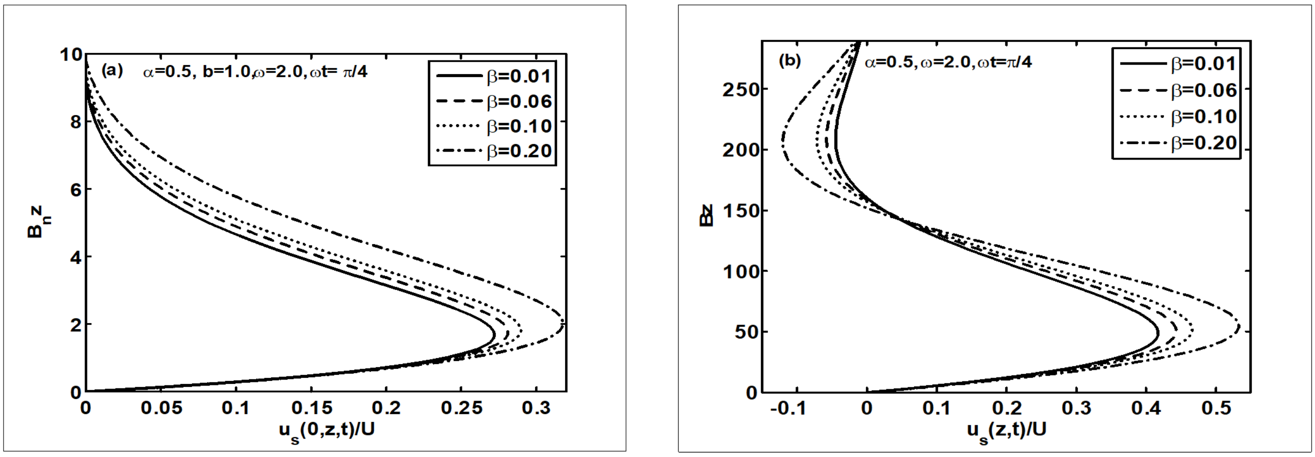

(a) (b)

Fig. 6. Profiles of the velocity u_s / U for different values of the rheological parameter β of the Burgers' fluid for the cosine oscillation: (a) presence of the side walls and (b) absence of the side walls.

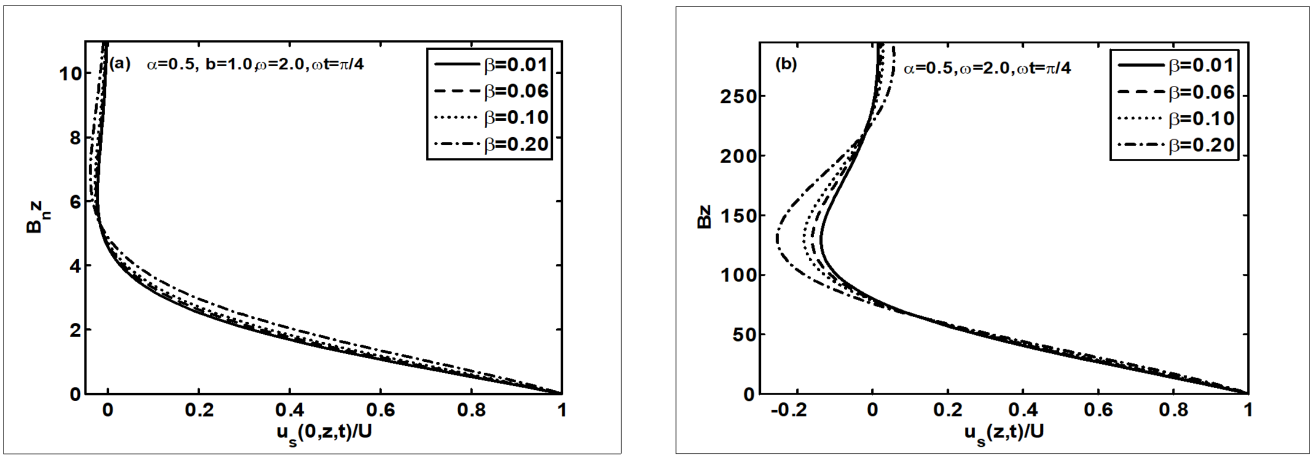

(a) (b)

Fig. 7. Profiles of the velocity u_s / U for different values of the rheological parameter β of the Burgers' fluid for the sine oscillation: (a) presence of the side walls and (b) absence of the side walls.

$$2A^2 = \frac{\omega\sqrt{\left(\lambda_r - \lambda - \lambda_r\gamma\omega^2\right)^2\omega^2 + \left(1 + (\lambda_r\lambda - \gamma)\omega^2\right)^2} + \left(\lambda_r - \lambda - \lambda_r\gamma\omega^2\right)\omega^2}{\nu\left(1 + \lambda_r^2\omega^2\right)},$$

$$2B^2 = \frac{\omega\sqrt{\left(\lambda_r - \lambda - \lambda_r\gamma\omega^2\right)^2\omega^2 + \left(1 + (\lambda_r\lambda - \gamma)\omega^2\right)^2} - \left(\lambda_r - \lambda - \lambda_r\gamma\omega^2\right)\omega^2}{\nu\left(1 + \lambda_r^2\omega^2\right)}.$$

The associated steady state solutions are

$$\frac{u_s(z,t)}{U} = \sum_{n=0}^{\infty}\frac{4(-1)^n}{(2n+1)\pi}e^{-Az}\cos(\omega t - Bz), \tag{41}$$

respectively,

$$\frac{u_s(z,t)}{U} = \sum_{n=0}^{\infty}\frac{4(-1)^n}{(2n+1)\pi}e^{-Az}\sin(\omega t - Bz). \tag{42}$$

4. Results and discussion

In the previous section, we have determined the exact solutions for the oscillating motion of a Burgers' fluid. To gain possession of some relevant physical aspects of the obtained results, several graphs for the steady-state velocity given by Eqs. (32), (33), (41) and (42) are plotted in this section. The graphs of $u_s(0,z,t)/U$ giving the velocity profiles at the middle of the channel in the presence of the side wall as well as $u_s(z,t)/U$ giving the velocity profiles corresponding to the motion over an infinite plate are drawn by assigning numerical values to different parameters involved. In addition, a comparison is made for different fluids for cosine oscillation in the presence of the side walls. These graphs have been plotted by introducing the following dimensionless quantities

$$u^* = \frac{u}{U},\ y^* = \frac{y}{\sqrt{\nu\lambda}},\ z^* = \frac{z}{\sqrt{\nu\lambda}},\ t^* = \frac{t}{\lambda},\ \omega^* = \lambda\omega,\ \alpha = \frac{\lambda_r}{\lambda}\ (<1),\ \beta = \frac{\gamma}{\lambda^2}\ \text{and}\ b^* = \frac{b}{\sqrt{\nu\lambda}},$$

where asterisks have been omitted for simplicity. Figures 2 and 3 depict the effect of time t on velocity profile in the presence as well as absence of the side walls for both cosine and sine oscillations of the bottom wall. Both oscillations have similar amplitudes, and a phase shift persists for all times. It clearly results from these figures that as the bottom plate starts oscillating, the velocity is developing and fluctuating around zero with the same frequency as the plate. Further, we can see that maximum amplitude of fluid oscillation occurs near the bottom plate and decreases far away from the plate. An inspection reveals that the velocity profiles are strongly influenced by the presence of the side walls. It is observed that the amplitudes of oscillations are smaller and approach to zero much earlier in the presence of the side walls as compared to those in the absence of the side walls. Moreover, boundary layer thickness is observed to be decreased in the presence of the side walls. This is due to increasing shearing force from the side walls. Hence, one can say that the flow driven over a flat plate in the presence of the side walls decays and approaches to zero much earlier than the flow over a flat plate in the absence of the side walls.

To see the effects of the elasticity parameter α on the velocity profiles, figures 4 and 5 are prepared for both cosine and sine oscillations of the boundary. The oscillatory nature of the flow is clearly observed from these figures. Figures 4 and 5 show that an increase in α induces a noticeable reduction in velocity for both type of oscillations across the channel. Further, it is apparent that velocity is strongly decreased in the presence of the side walls when compared to that in the absence of the side walls. Furthermore, the reduction in the velocity profile is accompanied by simultaneous reduction in the boundary layer thickness. These results are in accordance with the physical situations.

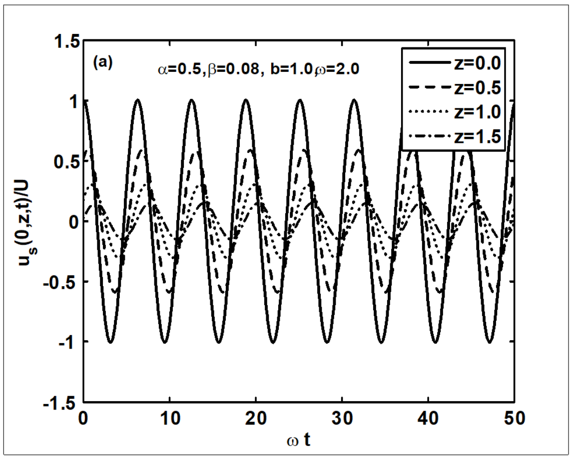

(a)

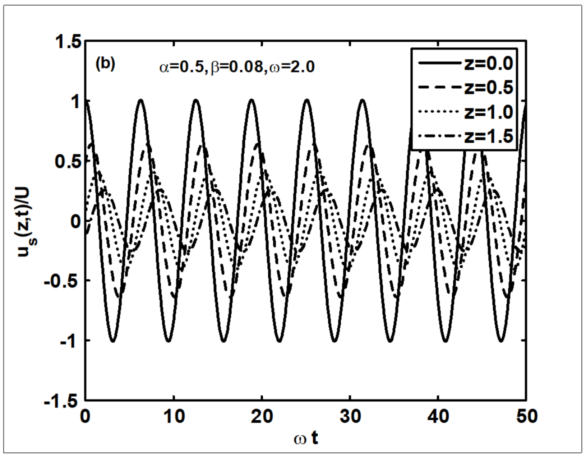

(b)

Fig. 8. Time series of the flow velocity for various z for the cosine oscillation: (a) presence of the side walls and (b) absence of the side walls.

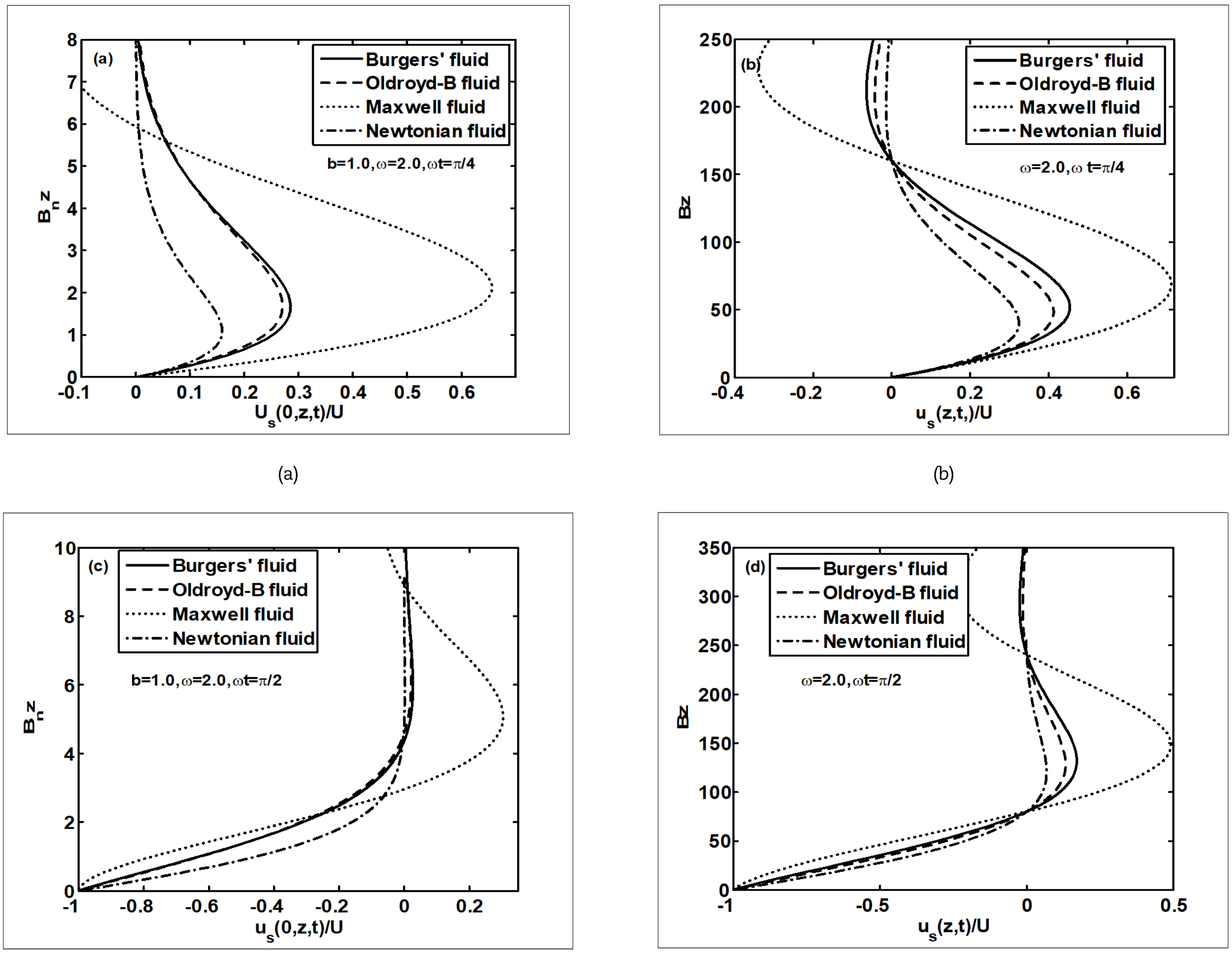

(a) (b) (c) (d)

Fig. 9. A comparison of profiles of the velocity u_s / U for different fluids for the cosine oscillation in the presence of the side walls (Burgers' fluid: $\beta = 0.08$, $\alpha = 0.5$; Oldroyd-B fluid: $\beta = 0.0$, $\alpha = 0.5$; Maxwell fluid: $\beta = 0.0$, $\alpha = 0.0$; Newtonian fluid: $\beta = 0.0$, $\alpha = 1.0$).

Figures 6 and 7 represent the velocity profiles for different values of rheological parameter β of the Burgers' fluid. The undulating nature of the flow evolution across the channel is clearly visible. By analyzing the graphs, it reveals that the velocity is a strong function of β. From these figures, it is apparent that a higher amplitude of the velocity fluctuation is observed to occur for larger values of β. We further infer from these figures that the effect of increasing the β is to thicker the boundary layer thickness. It is further noticeable that the amplitude of velocity and the boundary layer thickness are considerably greater in the absence of the side walls when compared with those in the presence of the side walls.

In figure 8 the velocity profiles are plotted for various values of z with the advancement of time. It is observed that the velocity fluctuates with time in a similar fashion as that of oscillations on the plate. An inspection shows that with an increase in z suppresses the amplitude of oscillation of the velocity.

Finally, for comparison, the profiles of the velocity corresponding to four models (Newtonian, Maxwell, Oldroyd-B and Burgers') are together depicted in figure 9 for the same values of times and the common material constants. The Maxwell fluid, as results from these figures, is the swiftest and the Newtonian is the slowest in the whole flow domain. Moreover, we noticed that the amplitude of velocity is slightly faster in the Burgers' fluid compared with the Oldroyd-B fluid.

5. Conclusion

In this study, we considered the oscillating flow of a Burgers fluid between two side walls over a plane wall. The motion of the fluid was induced by the oscillation of the bottom plate between two side walls perpendicular to the plate. The starting solutions were established using Fourier sine and Laplace transforms and again written as a sum of steady-state and transient solutions. It is worth pointing that in the absence of side wall, the obtained solutions can be easily reduced to those corresponding to the motion over an infinite plate. Also, the graphical results were plotted for the steady-state solutions in the presence as well as in the absence of side walls at the middle of the channel. Here, we have seen that the velocity and the boundary layer thickness were observed to decrease in the presence of the side walls. Also, an increase in the elasticity parameter α induced a noticeable reduction in velocity across the channel. Moreover, a higher amplitude of the velocity fluctuation was observed to occur for larger value of the rheological parameter β of the Burgers fluid. A comparison amongst different fluids models showed that the Maxwell fluid was the fastest and the Newtonian was the slowest in the whole domain. Furthermore, we have observed that the velocity was slightly faster in the Burgers fluid as compared with the Oldroyd-B fluid.

Appendix

In order to simplify the expressions of Eqs. (28) and (29), we have used the well-known integrals

$$\int_0^\infty \frac{(\xi^2+a^2)\xi\sin(\xi z)}{(\xi^2+a^2)^2+c^2}d\xi = \frac{\pi}{2}e^{-A_1 z}\cos(B_1 z), \tag{A1}$$

$$\int_0^\infty \frac{\xi\sin(\xi z)}{(\xi^2+a^2)^2+c^2}d\xi = \frac{\pi}{2c}e^{-A_1 z}\sin(B_1 z), \tag{A2}$$

where

$$2A_1^2 = \sqrt{a^4+c^2}+a^2, \quad 2B_1^2 = \sqrt{a^4+c^2}-a^2. \tag{A3}$$

Therefore, the following integral can be evaluated as

$$\begin{aligned}\int_0^\infty \psi_{3n}(\xi)\xi\sin(\xi z)d\xi &= \frac{\gamma(1+\omega^2(\lambda_r\lambda-\gamma))}{\nu^2(1+\lambda_r^2\omega^2)}\int_0^\infty \frac{\xi\sin(\xi z)d\xi}{\left(\xi^2+k_n^2+\frac{(\lambda_r-\lambda-\lambda_r\gamma\omega^2)\omega^2}{\nu(1+\lambda_r^2\omega^2)}\right)^2+\frac{\omega^2(1+(\lambda_r\lambda-\gamma)\omega^2)^2}{\nu^2(1+\lambda_r^2\omega^2)^2}} \\ &= \frac{\pi}{2}\frac{\gamma}{\omega\nu}e^{-A_n z}\sin(B_n z),\end{aligned} \tag{A4}$$

and

$$\begin{aligned}\int_0^\infty \psi_{4n}(\xi)\xi\sin(\xi z)d\xi &= -\frac{\gamma}{\nu}\int_0^\infty \frac{\left(\xi^2+k_n^2+\frac{(\lambda_r-\lambda-\lambda_r\gamma\omega^2)\omega^2}{\nu(1+\lambda_r^2\omega^2)}\right)\xi\sin(\xi z)d\xi}{\left(\xi^2+k_n^2+\frac{(\lambda_r-\lambda-\lambda_r\gamma\omega^2)\omega^2}{\nu(1+\lambda_r^2\omega^2)}\right)^2+\frac{\omega^2(1+(\lambda_r\lambda-\gamma)\omega^2)^2}{\nu^2(1+\lambda_r^2\omega^2)^2}} \\ &= -\frac{\pi}{2}\frac{\gamma}{\nu}e^{-A_n z}\cos(B_n z),\end{aligned} \tag{A5}$$

in which

$$2A_n^2 = \sqrt{\left(k_n^2+\frac{(\lambda_r-\lambda-\lambda_r\gamma\omega^2)\omega^2}{\nu(1+\lambda_r^2\omega^2)}\right)^2+\frac{\omega^2(1+(\lambda_r\lambda-\gamma)\omega^2)^2}{\nu^2(1+\lambda_r^2\omega^2)^2}}+\left(k_n^2+\frac{(\lambda_r-\lambda-\lambda_r\gamma\omega^2)\omega^2}{\nu(1+\lambda_r^2\omega^2)}\right), \tag{A6}$$

$$2B_n^2 = \sqrt{\left(k_n^2+\frac{(\lambda_r-\lambda-\lambda_r\gamma\omega^2)\omega^2}{\nu(1+\lambda_r^2\omega^2)}\right)^2+\frac{\omega^2(1+(\lambda_r\lambda-\gamma)\omega^2)^2}{\nu^2(1+\lambda_r^2\omega^2)^2}}-\left(k_n^2+\frac{(\lambda_r-\lambda-\lambda_r\gamma\omega^2)\omega^2}{\nu(1+\lambda_r^2\omega^2)}\right). \tag{A7}$$

Nomenclature

$\mathbf{V}$	Velocity Field	$u(y,z,t)$	Velocity Component in x-direction
t	Time	ν	Kinematic Viscosity
ρ	Density	U	Amplitude
p	Pressure	$H(.)$	Heaviside Unit Step Function
∇	Gradient Operator	$\bar{u}_n(\xi,t)$	Fourier Sine Transform of $u(z,t)$
$\mathbf{S}$	Extra Stress Tensor	$\bar{U}_n(\xi,q)$	Laplace Transform of $\bar{u}_n(\xi,t)$
μ	Dynamic Viscosity	$u_s(y,z,t)$	Steady-state Velocity
λ	Relaxation Time	$u_t(y,z,t)$	Transient Velocity
λ_r	Retardation Time	$\bar{U}(y,z,q)$	Laplace Transform of $u(y,z,t)$
$\mathbf{A}$	First Rivlin Ericksen Tensor	$\tau(y,z,t)$	Non-Trivial Shear Stress
$\mathbf{L}$	Velocity Gradient	$\bar{\tau}(y,z,q)$	Laplace Transform of $\tau(y,z,t)$

Author Contributions

S. Akram developed the mathematical modeling and suggested the solution of the problem; A. Anjum Solved the problem and drawn the graphical conclusion; M. Khan Wrote the manuscript. A. Hussain examined the theory validation. The manuscript was written through the contribution of all authors. All authors discussed the results, reviewed, and approved the final version of the manuscript.

Conflict of Interest

All authors declared that there is no conflict of interest of this research.

Funding

The authors received no financial support for the research, authorship, and publication of this article.

References

1. Rajagopal, K.R., Longitudinal and torsional oscillations of a rod in a non-Newtonian fluid, *Acta Mechanica*, 49(3-4), 1983, 281-285.
2. Bandelli, R., Rajagopal, K.R., Galdi, G.P., On some unsteady motions of fluids of second grade, *Archives of Mechanics*, 47, 1995, 661-676.
3. Erdogan, M.E., Plane surface suddenly set in motion in a non-Newtonian fluid, *Acta Mechanica*, 108(1-4), 1995, 179-187.
4. Asghar, S., Hayat, T., Siddiqui, A.M., Moving boundary in a non-Newtonian fluid, *International Journal of Non-Linear Mechanics*, 37(1), 2002, 75-80.
5. Fetecau, C., Fetecau, Corina., Starting solutions for some unsteady unidirectional flows of a second grade fluid, *International Journal of Engineering Science*, 43(10), 2005, 781-789.
6. Aksel, N., Fetecau, C., Scholle, M., Starting solutions for some unsteady unidirectional flows of Oldroyd-B fluids, *Zeitschrift für angewandte Mathematik und Physik* , 57(5), 2006, 815-831.
7. Hayat, T., Khan, M., Siddiqui A.M., Asghar, S., Transient flows of a second-grade fluid, *International Journal of Non-Linear Mechanics,* 39(10), 2004, 1621-1633.
8. Khan, M., Ali, S.H., Hayat, T., Fetecau, C., MHD flows of a second grade fluid between two side walls perpendicular to a plate through a porous medium, *International Journal of Non-Linear Mechanics,* 43(4), 2008, 302-319.
9. Khan, M., Ali, S.H., Qi, H.T., Exact solutions for some oscillating flows of a second grade fluid with a fractional derivative model, *Mathematical* and *Computer Modelling*, 49(7-8), 2009, 1519-1530.
10. Tan, W.C., Masuoka, T., Stokes' first problem for an Oldroyd-B fluid in a porous half space, *Physics of Fluids*, 17(2), 2005, 023101.
11. Burgers', J.M., Mechanical considerations-model systems-phenomenological theories of relaxation and of viscosity, in: J.M. Burgers (Ed.), First report on viscosity and plasticity, Nordemann Publishing Company, New York, 1935.
12. Lee, A.R., Markwick, A.H.D., The mechanical properties of bituminous surfacing materials under constant stress, *Journal of the Society of Chemical Industry*, 56, 1937, 146-156.
13. Tan, B.H., Jackson, I., Gerald, J.D.F., High-temperature viscoelasticity of fine-grained polycrystalline olivine, *Physics and Chemistry of Minerals,* 28(9), 2001, 641-664.
14. Peltier, W.R., Wu, P., Yuen, D.A., The viscosities of the earth mantle, in: F.D. Stacey, M.S. Paterson, A. Nicholas (Eds.), Anelasticity in the Earth, American Geophysical Union, Colorado, 1981.
15. Krishnan, J.M., Rajagopal, K.R., A thermodynamic framework for the constitutive modeling of asphalt concrete: theory and application, *Journal of Materials in Civil Engineering,* 16(2), 2004, 155-166.
16. Ravindran, P., Krishnan, J.M., Rajagopal, K.R., A note on the flow of a Burgers' fluid in an orthogonal rheometer, *International Journal* of *Engineering Science*, 42(19-20), 2004, 1973-1985.
17. Hayat, T., Hussain M., Khan, M., Effect of Hall current on the flows of a Burgers' fluid through a porous medium, *Transport* in *Porous Media,* 68(2), 2007, 249-263.
18. Fetecau, C., Vieru, D., Hayat, T., Fetecau, Corina, On the first problem of Stokes for Burgers' fluids, I. The case $\gamma < \lambda^2/4$, *Nonlinear* Analysis *Real World* Applications, 10(4), 2009, 2183-2194.
19. Khan, M., Ali, S.H., Fetecau, C., Exact solutions of accelerated flows for a Burgers' fluid. I. The case $\gamma < \lambda^2/4$, *Applied Mathematics* and *Computation*, 203(2), 2008, 881-894.
20. Hayat, T., Khan, S.B., Khan, M., Influence of Hall current on the rotating flow of a Burgers' fluid through a porous space, *Journal of Porous Media*, 11(3), 2008, 277-287.
21. Khan, M., Malik, R., Fetecau, Corina, Fetecau, C., Exact solutions for the unsteady flow of a Burgers' fluid between two side walls perpendicular to the plates, *Chemical Engineering Communications,* 197(11), 2010, 1367-1386.
22. Khan, M., Anjum A., Fetecau, C., On exact solutions of Stokes second problem for a Burgers' fluid, I. The case $\gamma < \lambda^2/4$, *Zeitschrift für angewandte Mathematik und Physik,* 61(4), 2010, 697-720.
23. Khan, M., Anjum A., Fetecau, C., Qi, H., Exact solutions for some oscillating motions of a fractional Burgers' fluid, *Mathematical and Computer Modelling*, 51(5-6), 2010, 682-692.
24. Aziz, T., Aziz, A., Khalique, C.M., Exact solutions for Stokes' flow of a non-Newtonian nanofluid Model: A lie similarity approach, *Zeitschrift für Naturforschung A*, 71(7), 2016, 621-630.
25. Aziz, T., Magan, A. B., Mahomed, F. M., Invariant solutions for the unsteady Magnetohydrodynamics (MHD) flow of a Fourth-grade fluid induced due to the impulsive motion of a flat porous plate, *Brazilian Journal of Physics*, 45(1), 2015, 120-131.
26. Griffiths, P. T., Non-Newtonian channel flow---exact solutions, *IMA Journal of Applied Mathematics*, 85(2), 2020, 263-279.
27. Sheikholeslami, M., Farshad, S.A., Shafee, A., Babazadeh, H., Performance of solar collector with turbulator involving nanomaterial turbulent regime, *Renewable Energy*, 163, 2021, 1222-1237.
28. Sheikholeslami, M., Farshad, S.A., Nanoparticle transportation inside a tube with quad-channel tapes involving solar radiation, *Powder Technology*, 378(A), 2021, 145-159.
29. Memon, K.N., Shah S. F., Siddiqui, A. M., Exact solution of unsteady tank drainage for Ellis fluid, *Journal of Applied Fluid Mechanics*, 11(6), 2018, 1629-1636.
30. Choi, D.S., Yun, S., Choi, W., An exact solution for Power-law fluids in a slit microchannel with different zeta potentials under electroosmotic forces, *Micromachines*, 9(10), 2018, 504.
31. Khan, M., Shahzad, A., Anjum, A., M. Mahomed, F., Analytic approximate solutions for time-dependent flow and heat transfer of a Sisko fluid, *International Journal of Numerical Methods for Heat & Fluid Flow*, 24(5), 2014, 1005-1019.
32. Menni, Y., Azzi, A., Chamkha, A.J., Aerodynamics and heat transfer over solid-deflectors in transverse, staggered, corrugated-upstream and corrugated-downstream patterns, *Periodica Polytechnica Mechanical Engineering*, 62(3), 2018, 209-217.
33. Akram, S., Nadeem, S., Hussain, A., Influence of lateral walls on peristaltic flow of a third grade fluid in a rectangular duct, *Journal of Applied Mechanical Engineering*, 3, 2014, 1-6.
34. Menni, Y., Chamkha, A.J., Lorenzini, G., Benyoucef, B., Computational fluid dynamics based numerical simulation of thermal and thermo-hydraulic performance of a solar air heater channel having various ribs on absorber plates, *Mathematical Modelling of Engineering Problems*, 6(2), 2019, 170-174.
35. Menni, Y., Azzi, A., Zidani, C., Benyoucef, B. ,Numerical analysis of turbulent forced-convection flow in a channel with staggered L-shaped baffles, *Journal of New Technology and Materials*, 6(2), 2016, 44-55.
36. Menni, Y., Chamkha, A.J., Azzi, A., Zidani, C., Numerical analysis of fluid flow and heat transfer characteristics of a new kind of vortex generators by comparison with those of traditional vortex generators, *International Journal of Fluid Mechanics Research*, 47(1), 2020, 23-42.
37. Menni, Y., Azzi, A., Chamkha, A.J., Turbulent heat transfer and fluid flow over complex geometry fins, *Defect and Diffusion Forum*, 38, 2018, 378-393.
38. Menni, Y., Azzi, A., Zidani, C., Use of waisted triangular-shaped baffles to enhance heat transfer in a constant temperature-surfaced rectangular channel, *Journal of Engineering Science and Technology*, 12(12), 2017, 3251-3273.
39. Menni, Y., Azzi, A., Chamkha, A.J., Developing heat transfer in a solar air channel with arc-shaped baffles: effect of baffle attack angle, *Journal of New Technology and Materials*, 8(1), 2018, 58-67.
40. Ahmed, A., Khan, M., Ahmed, J., Anjum, A., Nadeem, S., Mixed convective 3D flow of Maxwell nanofluid induced by stretching sheet: Application of Cattaneo-Christov theory, *Proceedings of the Institution of Mechanical Engineers, Part C: Journal of Mechanical Engineering Science*, 2020, 1-10.

ORCID iD

Safia Akram https://orcid.org/0000-0001-6288-6095
Asia Anjum https://orcid.org/0000-0002-1651-7851
M. Khan https://orcid.org/0000-0003-4404-1456
Anwar Hussain https://orcid.org/0000-0002-2571-8997

How to cite this article: Akram S., Anjum A., Khan M., Hussain A. On Stokes' Second Problem for Burgers' Fluid over a Plane Wall, *J. Appl. Comput. Mech.*, 7(3), 2021, 1514–1526. https://doi.org/10.22055/JACM.2020.35227.2603